

中国激光

扩展目标光子测距回波特性及误差研究

侯阿慧^{1,2*}, 胡以华^{1,2**}, 赵楠翔^{1,2***}, 方佳节^{1,2}, 张鑫源^{1,2}

¹ 国防科技大学脉冲功率激光技术国家重点实验室, 安徽 合肥 230037;

² 国防科技大学电子制约技术安徽省重点实验室, 安徽 合肥 230037

摘要 光子测距具有灵敏度高, 探测距离远的特点, 目标形状和姿态对光子测距的影响不可忽略。针对扩展平面、球面和非球面三种典型目标, 建立了扩展目标光子探测回波概率分布模型, 推导出不同倾斜角下混有时空分布的光子回波概率分布一般方程。实验表明, 扩展平面的光子回波概率分布与数值计算结果一致。理论仿真分析了扩展目标的光子回波概率分布特性, 讨论了光子测距误差与扩展目标类型和倾斜角间的变化规律。结果表明: 平均回波光子数为 3.9, 目标处激光光斑半径为 0.2 m, 倾斜角小于 20°时不同扩展目标间的光子测距误差小于 1.23 mm; 光子测距误差随着目标倾斜角的增大逐渐增大, 且扩展平面目标测距误差受倾斜角影响最大。

关键词 激光光学; 光子测距; 测距误差; 扩展目标; 概率分布; 回波特性

中图分类号 O439

文献标志码 A

doi: 10.3788/CJL202148.0401016

1 引言

光子计数激光雷达以灵敏度高、探测距离远和测距精度高的特点广泛应用于激光测距^[1-3]和目标探测^[4-5]领域。由于单光子探测器死时间的存在, 使得光子探测出现首光子偏置效应^[6], 导致光子回波概率分布产生较大畸变。在光子测距系统中, 回波光子数大小和激光回波脉宽的变化对光子测距误差影响尤为明显^[7-9]。Oh 等^[7]对光子测距误差进行了理论和实验对比, 首次提出了光子测距距离漂移误差, 研究了光子测距的误差和校正; 黄科等^[8]和 Chen 等^[9]深入分析了点目标的回波光子数和发射激光脉宽与光子测距误差的关系, 提出了校正补偿方法。上述研究侧重于分析光子探测系统发射端参数和点目标光子测距误差的关系, 未考虑面目标和体目标对光子测距误差的影响。目标形状差异和目标姿态变化会引起光子回波概率分布的畸变, 所导致的光子测距误差不容忽略。

李磊等^[10-11]分析了脉冲展宽和平面目标的倾斜角度间的关系, 并进行了激光测距回波实验验证, 但

未考虑发射激光空间强度分布对激光回波的影响; 徐孝彬等^[12-13]推导了平面目标的激光回波解析表达式, 分析了发射激光和目标参数对激光测距误差的影响。上述学者偏向于给出平面目标特定的回波表达式, 公式的普适性较弱, 忽略了三维目标的深度信息与激光测距误差的关系。谢庚承等^[14]研究了简单飞行目标的姿态变化与脉冲激光测距回波特性和测距误差的关系; Steinval^[15], Li 等^[16], Hao 等^[17], Xu 等^[18]对简单三维目标的脉冲激光回波分布进行了数值仿真和实验验证。上述研究主要是激光雷达直接探测模式下的目标特性和回波分布的关系分析, 强调目标特性对脉冲激光回波的调制作用, 缺乏光子探测模式下扩展目标的测距误差相关研究。

因此, 针对扩展平面、球面和非球面三种目标, 本文建立了扩展目标的光子探测回波概率模型, 推导了倾斜目标的光子回波概率分布方程; 通过实验验证了理论模型的正确性; 仿真对比分析了光子回波概率分布和激光脉冲回波特性的异同, 讨论了不同扩展目标的光子测距误差与目标倾斜角的变化规律。

收稿日期: 2020-07-01; 修回日期: 2020-07-29; 录用日期: 2020-08-20

基金项目: 国家自然科学基金(61871389)、国防科技大学科研计划项目(ZK18-01-02)

*E-mail: hou_a_hui068@163.com; **E-mail: skl_hyh@163.com; ***E-mail: southfly@163.com

2 光子探测回波概率分布模型

光子测距系统扩展目标的坐标系如图1所示,扩展目标中心位于坐标原点处,光子探测系统在 z 轴的负半轴,与原点的距离为 r_0 ,扩展目标相对于 z 轴的倾斜角度为 α 。发射激光服从三维高斯分布,为了准确描述发射激光的波形, z 轴传输波形采用重尾函数^[19]表示为

$$g(t) = \frac{2t}{\tau^2} \exp\left(-\frac{t^2}{\tau^2}\right), \quad (1)$$

式中: $\tau=W_{\text{FWHM}}/1.22$, W_{FWHM} 为发射激光的半峰全宽。

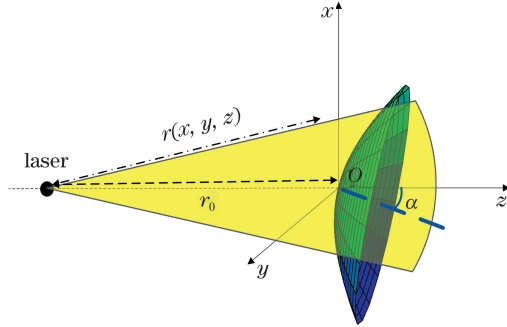


图1 光子测距扩展目标坐标系

Fig. 1 Coordinate system of photon ranging extended target

当激光垂直入射目标表面时^[13],单个目标面元的脉冲响应,可忽略脉冲展宽,仅考虑时间延迟和强度衰减,表示为

$$dh(t) = 4\pi\rho_0(x,y,z)g(x,y)g(t-t_0)\cos\beta dS, \quad (2)$$

$$\iint_{S_1} F[x, y, z(x, y)] dx dy = \iint_{S_2} F[x(x_0, y_0), y(x_0, y_0), z(x, y)] |\mathbf{J}| dx_0 dy_0, \quad (5)$$

式中: $|\mathbf{J}|$ 为雅克比行列式, $|\mathbf{J}| = \begin{vmatrix} \partial x / \partial x_0 & \partial x / \partial y_0 \\ \partial y / \partial x_0 & \partial y / \partial y_0 \end{vmatrix}$ 。

最终实现不同倾斜角的目标回波计算。

因此,在第 i th时间栅格内的平均信号回波光

式中: $\rho_0(x, y, z)$ 为目标的反射率; t_0 为面元的时间延迟, $t_0 = 2r(x, y, z)/c$, c 为光速; β 为面元法线与激光传输方向的夹角; $g(x, y)$ 为发射激光在 xoy 面的能量分布。 $g(x, y)$ 表示为

$$g(x, y) = \frac{2P}{\pi\omega^2} \exp\left(-2\frac{x^2+y^2}{\omega^2}\right), \quad (3)$$

式中: P 为激光总功率; ω 为面元处激光光斑半径, $\omega = \omega_0 \sqrt{1 + [\lambda(z+r_0)/\pi\omega_0^2]^2}$, ω_0 为发射激光的束腰半径, $\omega_0 = 2\lambda/\pi\varphi_0$, φ_0 为发射激光发散角。

则整个目标的脉冲响应为所有单元面积的积分,即 $h(t) = \iint_S dh(t)$,目标的回波波形信号最终表示^[18]为

$$L(t) = T_0^2 \eta_t \eta_r \eta_q \frac{A_r \cos \alpha}{\pi r_0^2} \iint_S 4\pi \rho_0(x, y, z) \times g(x, y) g(t - t_0) \cos \beta dS, \quad (4)$$

式中: T_0 为大气单程通过率; η_t 和 η_r 分别为发射和接收系统的系统效率; η_q 为单光子探测器的探测效率; A_r 为探测系统的接收面积。

目标发生姿态的变化,采用坐标变换的方法进行求解,当目标的倾斜角为 α ,即目标绕 y 轴旋转

时,其变换矩阵 $\mathbf{R} = \begin{pmatrix} \cos \alpha & 0 & \sin \alpha \\ 0 & 1 & 0 \\ -\cos \alpha & 0 & \sin \alpha \end{pmatrix}$,设旋转后的坐标 $\mathbf{s} = (x, y, z)$,旋转前的坐标 $\mathbf{s}_0 = (x_0, y_0, z_0)$,则 $\mathbf{s} = \mathbf{R}\mathbf{s}_0$ 。结合二重积分的换元定理,旋转后的回波分布可用垂直入射得到回波进行转换,表示为

子数 $N_s(i) = \int_{t_i} L(t) dt/hv$, hv 为单光子能量。基于单光子探测器的泊松响应分布模型^[20-21],受死时间的影响^[22-23],光子测距激光雷达在第 i th时间栅格的探测概率^[20]为

$$P(i) = \begin{cases} \{1 - \exp[-N(i)]\} \times \exp\left[-\sum_{j=1}^{i-1} N(j)\right], & i < d_{\text{dead}} \\ \{1 - \exp[-N(i)]\} \times \left[1 - \sum_{j=i-d_{\text{dead}}+1}^{i-1} P(j)\right], & i \geq d_{\text{dead}} \end{cases}, \quad (6)$$

式中: $N(i)$ 为第 i th时间栅格内的平均回波光子数, $N(i) = N_s(i) + N_n$, N_n 为单个时间栅格的平

均噪声光子数; $d_{\text{dead}} = \text{Ceiling}(T_{\text{dead}}/\delta t)$, T_{dead} 为死时间, δt 为时间栅格的宽度,Ceiling为向上取

整;第二项是第 i th 时间栅格的前面 $i - 1/d_{\text{dead}}$ 个栅格内探测器都未被触发的概率。因为目前光子计数激光雷达的单光子探测器死时间相对较长,且测距系统一般为一次探测一次触发以防止距离模糊,因此本文主要分析单触发模式^[22]下的光子测距性能。由此,求得光子测距的回波概率分布。

基于时间相关光子计数器(TCSPC)得到的光子测距回波概率分布,结合质心算法^[8-9],可得光子探测的时间均值 \bar{t} 和发射激光的时间均值 \bar{t}_0 ,分别表示为

$$\bar{t} = \frac{\sum_{T_p} P(i) t_i}{\sum_{T_p} P(i)}, \quad \bar{t}_0 = \frac{\int g(t) t dt}{\int g(t) dt}. \quad (7)$$

光子探测的光子回波概率分布相较于激光脉冲回波前移的距离定义为光子测距的距离漂移 R_{we} ^[7],表示为

$$R_{\text{we}} = \frac{c}{2} (\bar{t} - \bar{t}_0 - 2r_0/c). \quad (8)$$

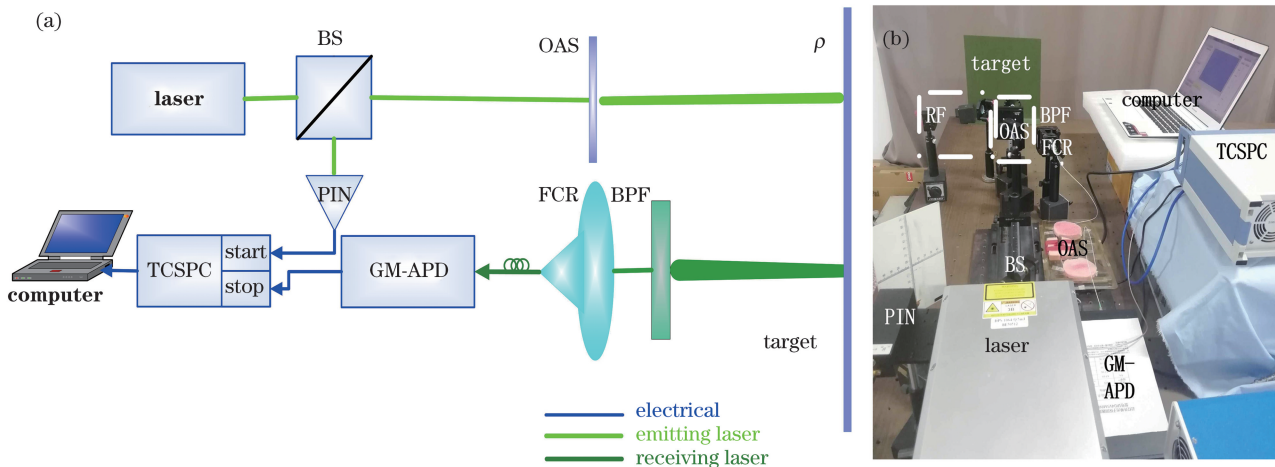


图2 光子测距系统。(a)光子测距系统示意图;(b)光子测距系统现场实验图

Fig. 2 Photon ranging system. (a) Schematic of photon ranging system; (b) experimental diagram of photon ranging system

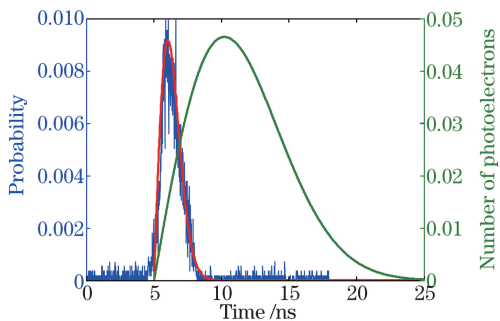


图3 扩展平面的光子测距实验结果

Fig. 3 Experimental results of photon ranging of extended flat

3 实验与光子测距误差分析

为验证模型推导理论的正确性,搭建了光子计数激光雷达测距系统,进行了扩展平面目标光子测距实验,获得了扩展平面的光子回波概率分布。脉冲激光波长为 1064 nm,单脉冲能量为 5 μJ ,脉宽为 9 ns,目标与光束垂直,时间栅格为 16 ps,光子测距系统示意图和光子测距系统的现场图如图 2 所示,图中 BS 为分束器,OAS 为衰减器,BPF 为滤波片,FCR 为光纤耦合器,GM-APD 为近红外单光子探测器,TCSPC 为时间相关光子计数器。图 2(b)中添加了反射镜组(RF)以增加探测距离,在接收端添加了一个光纤衰减器使得回波信号在光子级别。扩展平面光子回波概率分布的实验结果和数值计算结果如图 3 所示,实际的回波光子探测概率分布与理论结果基本一致。在实际的探测中,会受到周围环境的抖动影响,使得光子回波概率分布前端出现抖动,时间栅格较小,在累积次数有限的情况下,光子累积探测概率分布的毛刺较多。

3.1 扩展目标的回波特性分析

扩展目标可分为平面、球面和非球面三大类。扩展目标的不同样式会导致激光测距和光子测距产生误差,设置光子计数激光雷达的时间栅格为 16 ps,发射激光半峰全宽为 100 ps,单脉冲能量为 1 nJ,发散角为 0.02 mrad,探测距离为 10 km,扩展目标为朗伯体,反射率为 0.9。

扩展平面采用直角坐标系进行求解,平面目标的不同倾斜角的雅克比行列式 $|J| = \cos \alpha$ 。球面和非球面采用柱状坐标系,球面的雅克比行列式

$|J| = \rho \cos \alpha + \rho^2 \cos \theta \sin \alpha (R_s^2 - \rho^2)^{-1/2}$, 式中 R_s 为球面的曲率半径。复杂目标非球面^[17]的表达式为

$$z = \frac{CS^2}{1+B} + A_1 S^4 + A_2 S^6 + A_3 S^8 + A_4 S^{10}, \quad (9)$$

式中: $C=1/R_0$, R_0 为曲面顶点处的曲率半径; $S^2=x^2+y^2$; $B=\sqrt{1-(K+1)C^2S^2}$, K 为偏心率函数; A_1, A_2, A_3, A_4 为非球面的形变参数。则非球面的雅克比行列式为 $|J| = \rho \cos \alpha + \rho \cos \theta \sin \alpha [2C\rho(1+B) + C^3\rho^3(K+1)B/(1+B)^2 + 4A_1 S^3 + 6A_2 S^5 + 8A_3 S^7 +$

$10A_4 S^9]$ 。本文假设 $K=-2, R_0=2, A_1=0.05, A_2=10^{-3}, A_3=10^{-5}, A_4=10^{-6}$ 。三种扩展目标不同倾角的直接探测激光脉冲回波和光子计数激光雷达的光子回波概率分布如图 4 所示。直接探测工作在线性模式, 单次探测即可得到目标的脉冲激光回波; 光子探测工作在盖革模式, 通过多次累积探测, 得到回波光子的概率统计直方图。为便于分析, 将脉冲激光回波用光电子数表示, 其中图 4(a)、(c)、(e) 为直接探测的激光脉冲回波, 纵坐标为光电子数; 图 4(b)、(d)、(f) 为光子回波概率分布, 纵坐标为光子探测的雪崩概率。

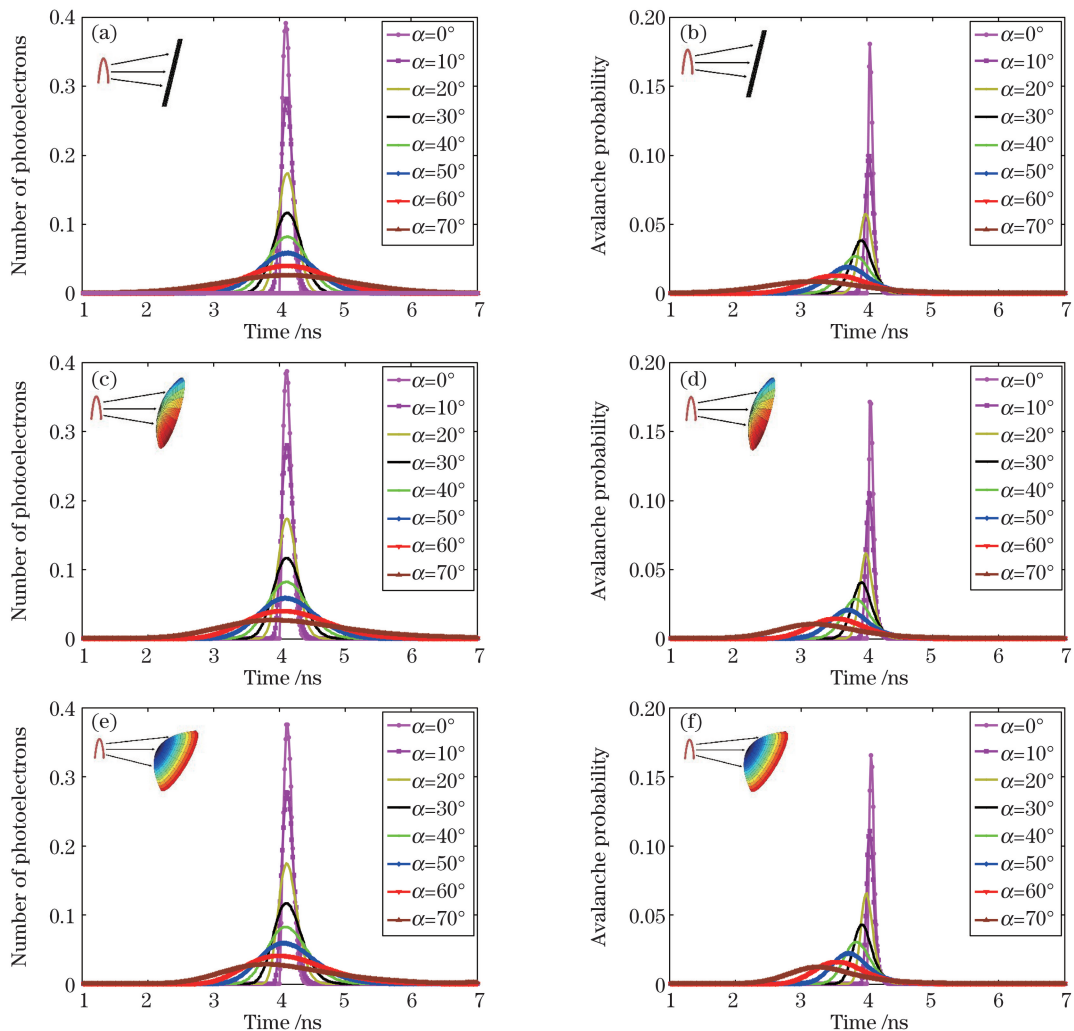


图 4 扩展目标的激光脉冲回波和光子回波概率分布。(a)(b)扩展平面;(c)(d)扩展球面;(e)(f)扩展非球面

Fig. 4 Laser pulse echo and photon echo probability distribution of extend targets. (a)(b) Extended flat; (c)(d) extended sphere; (e)(f) extended aspheric

如图 4 所示, 随着倾斜角 α 的增大, 扩展目标的激光脉冲回波脉宽变宽, 峰值降低, 相较于调 Q 发射激光, 激光脉冲回波的前端更加平缓; 扩展平面

目标在激光脉冲回波波形上服从高斯分布, 中心位置不变; 当倾斜角较大时, 球面和非球面的回波波形发生畸变, 重心产生一定的前移。光子回波概率分

布与回波的强度和脉宽有较大的关系^[9],由于单光子探测器死时间的存在,光子探测存在首光子效应^[6],扩展目标的倾斜角越大,目标的激光脉冲回波脉宽越宽,光子回波概率分布前移越大,光子回波概率分布的方差也越大。相较于扩展球面和非球面目标,扩展平面目标的光子回波概率分布前移最大,且方差偏大。综上,相较于激光脉冲回波,光子测距产生的光子回波概率分布存在较大的波形前移,概率

分布方差更小。

3.2 扩展目标的测距误差分析

为定量描述不同扩展目标的姿态对光子测距的影响,利用质心算法获得目标的测量距离,平面、球面和非球面三种扩展目标的距离漂移误差如图5所示。PIN二极管探测的发射信号波形质心为参考时刻,目标的脉冲激光回波的质心为直接探测的时刻点,回波光子概率分布的质心则对应光子测距的时刻点。

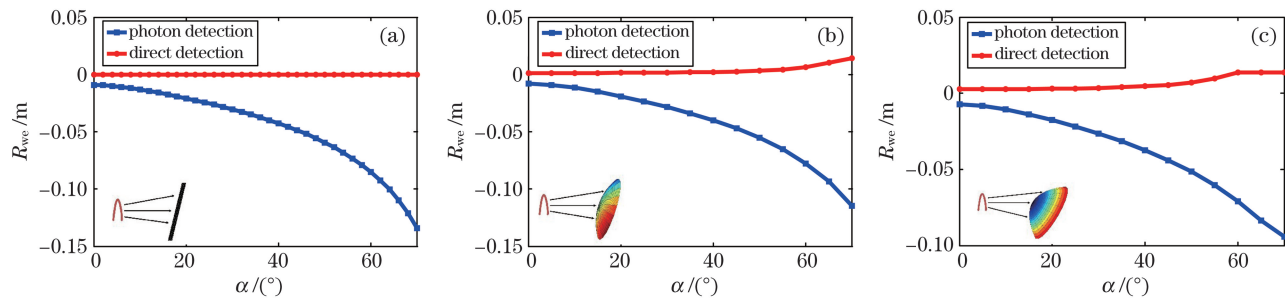


图5 扩展目标的距离漂移误差。(a)平面;(b)球面;(c)非球面

Fig. 5 Distance drift error of extended targets. (a) Flat; (b) sphere; (c) aspheric

如图5所示,不同扩展目标的直接探测测距结果几乎与目标的姿态倾斜角度无关,光子测距的距离漂移随倾斜角的增大而增大。仿真设置到达目标光斑直径约为0.2 m,当目标的旋转角度为70°时,扩展平面激光脉冲回波的脉宽约为2 ns,略大于扩展球面和非球面目标,三种扩展目标的质心仍在真实距离附近,采用质心算法求解,三种扩展目标的直接探测最大测距误差为1.4 cm,甚至随着倾斜角的变化,扩展平面目标的测距误差始终为0。光子测距的测距误差随着扩展目标姿态倾斜角的增大而逐渐增大,当目标倾斜角为0°时,光子探测相较于直接探测仍存在一定的测距误差,为了更好地分析不同扩展目标的光子测距误差的来源,不同目标的单脉冲的平均回波光子数如表1所示。可知,扩展目

标的平均回波光子数约为3.9,扩展球面和非球面的平均回波光子数略大于扩展平面;倾斜角为70°时,扩展球面和非球面存在微弱遮挡效应,平均回波光子数减小,但光子探测平均回波整体上还是在3.9附近。由(8)式可知,当回波光子数波动小于0.1时,激光脉宽为2 ns,光子数变化引起的距离漂移小于0.8 mm,因此光子测距误差主要来源于扩展目标姿态变化引起的回波波形变化。目标扩展角越大,脉宽越宽,光子测距前移的距离漂移越大,光子测距的误差也就越大。因此在后续的光子测距误差分析中,以目标倾斜角为0°时的光子探测距离为 R_{we}^0 参考标准,即光子探测测距误差可由光子探测的距离漂移表示为

$$R_b = R_{we} - R_{we}^0 \quad (10)$$

表1 扩展目标不同倾斜角的平均回波光子数

Table 1 Average number of photon echo at different tilt angles of extended targets

Target	Angle / (°)							
	0	10	20	30	40	50	60	70
Flat	3.8886	3.8975	3.8976	3.8975	3.8975	3.8973	3.8975	3.8974
Sphere	3.9082	3.9088	3.9095	3.9108	3.9127	3.9160	3.9213	3.8868
Aspheric	3.9082	3.9077	3.9084	3.9098	3.9117	3.9147	3.9079	3.8352

三种扩展目标的光子测距误差变化趋势相似,为进一步对比不同扩展目标的测距性能,其测距误差的结果如图6所示。

由图6可知,扩展目标的光子测距误差随倾斜

角的增大呈近似指数增大,当倾斜角小于20°时,扩展目标的光子测距误差在1.1 cm左右,平面、球面和非球面三种扩展目标间的光子测距误差差值小于1.23 mm,因而一般情况下可忽略不同扩展目标类

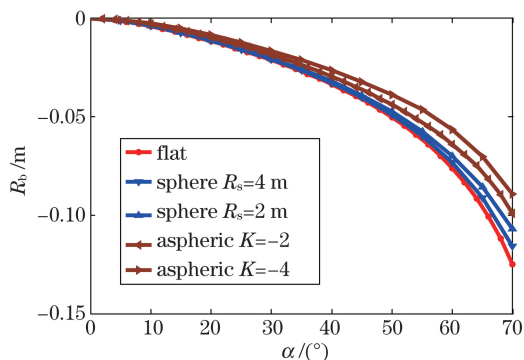


图 6 扩展目标的光子测距误差

Fig. 6 Photon ranging error of extended targets

型带来的光子测距误差;当倾斜角大于 20° 时,平面目标的光子测距精度受倾斜角的影响最大,非球面受倾斜角的影响最小,当目标倾斜角为 70° 时,扩展平面的光子测距误差达到 12.5 cm ,扩展非球面的光子测距误差为 8.9 cm 。随着球面曲率半径的增大,扩展球面光子测距误差逐渐增大,逼近平面的测距误差;非球面的偏心率参数的绝对值越大,光子测距误差随倾斜角的变化越小。综上,扩展目标的光子测距误差主要与目标姿态引起的波形变化有关,平面目标的光子测距误差受倾斜角的影响最大,非球面最小;当倾斜角小于 20° 时,扩展目标的光子测距与扩展目标的形状几乎无关。

4 结 论

本文建立了扩展目标光子探测回波概率模型,利用扩展目标的反射特性、目标形状及倾斜角等信息,推导了光子回波概率分布方程。该模型亦适用于非扩展目标。通过搭建扩展平面的光子测距实验系统,验证了模型的正确性。对比分析了光子回波概率分布与激光脉冲回波间的异同,在此基础上,讨论了扩展平面、球面和非球面三种目标的光子测距误差与倾斜角间的变化规律。结果表明:相较于激光脉冲回波,光子回波概率分布随着倾斜角的增大整体前移,方差增加幅度较小;基于质心算法,直接探测距离误差随扩展目标姿态倾斜角的变化幅度较小,最大测距误差为 1.4 cm ,相较于光子测距误差,其可忽略不计;光子测距的误差随着目标倾斜角的增大逐渐增大,扩展平面目标受倾斜角影响最大,可达 12.5 cm ;当倾斜角小于 20° 时,扩展目标的光子测距与扩展目标的形状几乎无关。这些结论为光子测距性能和误差分析提供了理论依据,为测距误差修正和性能提升提供了可靠的信息支撑。进一步

地,结合文中的光子回波概率分布方程与实际光子回波测量结果,亦可反演出扩展目标的姿态信息。

参 考 文 献

- [1] Luo Y, He Y, Geng L M, et al. Long-distance laser ranging lidar based on photon counting technology[J]. Chinese Journal of Lasers, 2016, 43(5): 0514001. 罗远, 贺岩, 耿立明, 等. 基于光子计数技术的远程测距激光雷达[J]. 中国激光, 2016, 43 (5): 0514001.
- [2] Huang K, Li S, Ma Y, et al. Detection probability model of single-photon laser altimetry and its range accuracy[J]. Chinese Journal of Lasers, 2016, 43 (11): 1110001. 黄科, 李松, 马跃, 等. 单光子模式激光测高探测概率模型与精度分析[J]. 中国激光, 2016, 43(11): 1110001.
- [3] Liu H B, Li M, Shu R, et al. Estimation and verification of high-accuracy laser ranging on several photons[J]. Infrared and Laser Engineering, 2019, 48(1): 0106001. 刘鸿彬, 李铭, 舒嵘, 等. 少光子灵敏度精密激光测距方法及验证[J]. 红外与激光工程, 2019, 48(1): 0106001.
- [4] Ding Y X, Li Y F, Liu H B, et al. Photon counting experiment based on InGaAs detector in daylight[J]. Chinese Journal of Lasers, 2018, 45(11): 1104003. 丁宇星, 李永富, 刘鸿彬, 等. 基于 InGaAs 探测器的日光条件光子计数实验[J]. 中国激光, 2018, 45 (11): 1104003.
- [5] Pawlikowska A M, Halimi A, Lamb R A, et al. Single-photon three-dimensional imaging at up to 10 kilometers range[J]. Optics Express, 2017, 25(10): 11919-11931.
- [6] Barton-Grimley R A, Thayer J P, Hayman M. Nonlinear target count rate estimation in single-photon lidar due to first photon bias [J]. Optics Letters, 2019, 44(5): 1249-1252.
- [7] Oh M S, Kong H J, Kim T H, et al. Reduction of range walk error in direct detection laser radar using a Geiger mode avalanche photodiode [J]. Optics Communications, 2010, 283(2):304-308.
- [8] Huang K, Li S, Ma Y, et al. Theoretical model and correction method of range walk error for single-photon laser ranging[J]. Acta Physica Sinica, 2018, 67(6): 064205. 黄科, 李松, 马跃, 等. 单光子激光测距的漂移误差理论模型及补偿方法[J]. 物理学报, 2018, 67(6): 064205.
- [9] Chen Z D, Li X D, Li X H, et al. A correction

- method for range walk error in time-correlated single-photon counting using photomultiplier tube [J]. Optics Communications, 2019, 434:7-11.
- [10] Li L, Hu Y H, Zhao N X, et al. Experiment on the stretching characteristics of pulse width of laser remote sensing echo [J]. Infrared and Laser Engineering, 2010, 39(2): 246-250.
李磊, 胡以华, 赵楠翔, 等. 激光遥感目标回波脉宽展宽特性实验[J]. 红外与激光工程, 2010, 39(2): 246-250.
- [11] Zhao N X, Hu Y H, Lei W H, et al. Small target imaging method based on the laser echo waveform analysis[J]. Infrared and Laser Engineering, 2009, 38(4): 748-752.
赵楠翔, 胡以华, 雷武虎, 等. 激光回波波形分析小目标检测成像方法[J]. 红外与激光工程, 2009, 38(4): 748-752.
- [12] Xu X B, Zhang H, Zhang X J, et al. Effect of plane target characteristics on ranging distribution for pulse laser detection [J]. Acta Physica Sinica, 2016, 65(21): 210601.
徐孝彬, 张合, 张祥金, 等. 脉冲激光探测平面目标特性对测距分布的影响[J]. 物理学报, 2016, 65(21): 210601.
- [13] Xu X B, Zhang H, Chen S S. Plane target echo characteristics of pulsed laser circular-viewing detection [J]. Acta Optica Sinica, 2017, 37(4): 0414003.
徐孝彬, 张合, 陈杉杉. 脉冲激光周向探测平面目标回波特性[J]. 光学学报, 2017, 37(4): 0414003.
- [14] Xie G C, Ye Y D, Li J M, et al. Echo characteristics and range error for pulse laser ranging [J]. Chinese Journal of Lasers, 2018, 45(6): 0610001.
谢庚承, 叶一东, 李建民, 等. 脉冲激光测距回波特性及测距误差研究[J]. 中国激光, 2018, 45(6): 0610001.
- [15] Steinvall O. Effects of target shape and reflection on laser radar cross sections [J]. Applied Optics, 2000, 39(24): 4381-4391.
- [16] Li Y, Wu Z. Targets recognition using subnanosecond pulse laser range profiles [J]. Optics Express, 2010, 18(16): 16788-16796.
- [17] Hao Q, Cheng Y, Cao J, et al. Analytical and numerical approaches to study echo laser pulse profile affected by target and atmospheric turbulence [J]. Optics Express, 2016, 24(22): 25026-25042.
- [18] Xu X B, Zhang H, Luo M Z, et al. Research on target echo characteristics and ranging accuracy for laser radar [J]. Infrared Physics & Technology, 2019, 96:330-339.
- [19] Xu L, Zhang Y, Zhang Y, et al. Signal restoration method for restraining the range walk error of Geiger-mode avalanche photodiode lidar in acquiring a merged three-dimensional image [J]. Applied Optics, 2017, 56(11): 3059-3063.
- [20] Fouche D G. Detection and false-alarm probabilities for laser radars that use Geiger-mode detectors [J]. Applied Optics, 2003, 42(27): 5388-5398.
- [21] Degnan J J. Photon-counting multikilohertz microlaser altimeters for airborne and spaceborne topographic measurements [J]. Journal of Geodynamics, 2002, 34(3/4):503-549.
- [22] Gatt P, Johnson S, Nichols T. Dead-time effects on Geiger-mode APD performance [J]. Proceedings of SPIE, 2007, 6550: 65500I.
- [23] Li Z, Lai J, Wang C, et al. Influence of dead-time on detection efficiency and range performance of photon-counting laser radar that uses a Geiger-mode avalanche photodiode [J]. Applied Optics, 2017, 56(23): 6680-6687.

Echo Characteristics and Error of Extended Target for Photon Ranging

Hou Ahui^{1,2*}, Hu Yihua^{1,2**}, Zhao Nanxiang^{1,2***}, Fang Jiajie^{1,2}, Zhang Xinyuan^{1,2}

¹ State Key Laboratory of Pulsed Power Laser (National University of Defense Technology),
Hefei, Anhui 230037, China;

² Anhui Key Laboratory of Electronic Restriction (National University of Defense Technology),
Hefei, Anhui 230037, China

Abstract

Objective Photon ranging exhibits the advantages of high sensitivity and long-distance detection. Compared with laser ranging in the linear mode, the photon detection exhibits the first photon bias effect owing to the dead-time of the single-photon detector, which results in greater distortion of the probability distribution of photon echo. This distortion is closely related to the intensity and distribution of the laser echo. There is a close relationship between

the target shape and posture and the probability distribution of photon echo. As a result, the range errors in photon ranging caused by the target shape and posture cannot be ignored. Most researchers have focused on analyzing the modulation effect of target characteristics on the laser pulse echo. However, there is a lack of research on the range errors of extended targets in the photon-detection mode. Therefore, we discuss the relationship between the target shape and inclination and photon ranging for three typical extended targets.

Methods Based on the Poisson probability response model and the traditional laser radar equation, the probability distribution model for the photon detection of an extended target is established herein. Combining this with the coordinate-rotation transformation formula, the general probability distribution equation mixed with spatial and temporal distribution at different inclinations is derived for the three typical extended targets: a plane, a sphere, and an aspheric. Experimental results reveal that the probability distribution of this photon echo is consistent with the numerical results. We then simulate and analyze the differences in the photon echo probability distribution and laser pulse echo characteristics of the three typical extended targets. Finally, the variation between the range errors in photon detection and the types and inclinations of the extended targets is discussed theoretically.

Results and Discussions Compared with the laser pulse echo, the probability distribution of the photon echo moves forward as the inclination increases, and the variance decreases. At the same time, the pulse width of the laser echo modulated by the extended plane is wider than those of the extended spherical and aspherical surfaces. Furthermore, the probability distribution of the photon echo of the extended plane moves forward the most. The photon ranging error of the extended targets exponentially increases with the increase in inclination. The average number of echo photons is 3.9, the laser spot radius of the target is 0.2 m, and when the inclination is less than 20°, the difference in the photon ranging errors between the three extended targets is less than 1.23 mm. As a result, the range errors in the photon detection caused by different extended target types could be ignored. In addition, when the inclination is greater than 20°, the photon ranging accuracy of the extended plane is most affected by the inclination, whereas that of the aspheric surface is the least affected. When the target inclination is 70°, the photon ranging errors for the extended plane and spherical and aspheric surfaces are 12.5 cm, 10.6 cm, and 8.9 cm, respectively.

Conclusions Based on the center-of-mass detection method, the range errors in the direct detection vary slightly with the inclination of the extended targets, which is negligible compared with those in photon ranging. The range errors in photon detection increase as the inclination of the target increases. The photon-ranging errors for the extension plane are most affected by the inclination. If the inclination was smaller, the photon ranging of the extended target would be almost independent of the shapes of the extended targets. These conclusions provide a theoretical basis for the photon ranging performance and error analysis and provide a reliable information support for range-error correction and performance improvement. Furthermore, the posture information of the extended target can be acquired by combining the equation of photon echo probability distribution with the measurement results of the photon echo.

Key words laser optics; photon ranging; range error; extended target; probability distribution; echo characteristics

OCIS codes 140.3538; 280.3640; 250.0040; 270.5290